RSC Advances

PAPER

View Article Online
View Journal | View Issue

Cite this: *RSC Adv.*, 2020, **10**, 23916

Surface coating determines the inflammatory potential of magnetite nanoparticles in murine renal podocytes and mesangial cells†

Michal Selc,[ab] Filip Razga,[cd] Veronika Nemethova,[cd] Petra Mazancova,[cd] Monika Ursinyova,[e] Marta Novotova,[f] Kristina Kopecka,[a] Alena Gabelova[a] and Andrea Babelova *[ab]

Drug-induced nephrotoxicity is a frequent adverse event and a dose-limiting factor in patient treatment and is a leading cause of prospective drug attrition during pharmaceutical development. Despite the obvious benefits of nanotherapeutics in healthcare strategies, the clearance of imaging agents and nanocarriers from the body following their therapeutic or diagnostic application generates concerns about their safety for human health. Considering the potency of nanoparticles and their massive utilization in biomedicine the impact of magnetic nanoparticles (MNPs) on cells forming the filtration apparatus of the kidney was studied. Using primary mouse renal glomerular podocytes and mesangial cells, we investigated their response to exposure to magnetic nanoparticles coated with polyethylene glycol and bovine serum albumin. Cultured podocytes were more sensitive to MNPs than mesangial cells displaying signs of cell damage and stronger inflammatory response. Both types of MNPs induced the remodeling of actin fibers, affected the cell shape and triggered expression of inflammatory cytokines TNFα and IL-6 in podocytes. On the other hand, iNOS was induced in both renal cell types but only by MNPs with a polyethylene glycol coating. Our results have revealed that the type of cell and the type of nanoparticle coating might be the strongest determinants of cellular response toward nanoparticle exposure. Differences in susceptibility of cells to MNPs might be evident also between neighboring renal cell subpopulations integrally forming functional sub-units of this organ.

Received 7th April 2020
Accepted 16th June 2020

DOI: 10.1039/d0ra03133j

rsc.li/rsc-advances

Introduction

The kidneys are unique organs characterized by a high degree of heterogeneity.[1] To sustain the main function of the kidneys in terms of osmoregulation and maintaining body fluid homeostasis, they need to remove a number of waste products and toxins in the urine and reabsorb water and electrolytes.[2] To achieve proper blood clearance, different types of cells with precisely defined functions are engaged which underlies their inherent sensitivity to potentially toxic substances.[3] Owing to the naturally high blood supply and the ability to concentrate toxins, kidney cells are particularly exposed to xenobiotics.[4] The filtration apparatus, so called glomerulus, is complex and its integrity is maintained by a close interplay of all participating cell types and constituents.[5] Mesangial cells provide support for the glomerular capillaries, help to regulate the filtration process, regulate glomerular hemodynamics and elasticity[6] and by increase in extracellular matrix synthesis they may contribute to development of interstitial fibrosis.[7–9] Terminally differentiated and non-proliferating podocytes are highly specialized epithelial cells that constitute essential component of the renal filtration barrier and by forming filtration slits with their foot processes enwrapping glomerular capillaries they prevent the loss of serum proteins into urine.[5,10–12] Injury of podocytes is manifested by structural change of podocyte cell shape, so called "foot process effacement" that is a hallmark of proteinuric renal diseases.[13] Given their exceedingly complex structure, even minor changes in actin cytoskeleton lead to podocyte damage.[14] Signals from damaged podocytes to the mesangium, or the hemodynamic factors triggered by podocyte loss, provide stimuli to the mesangial cells to enhance ECM synthesis.[15]

[a]*Department of Nanobiology, Cancer Research Institute, Biomedical Research Center, Slovak Academy of Sciences, Dubravska Cesta 9, 84505 Bratislava, Slovak Republic. E-mail: andrea.babelova@savba.sk; Fax: +421-2-5477-4284; Tel: +421-2-322-95189*

[b]*Centre for Advanced Material Application, Slovak Academy of Sciences, Dubravska Cesta 9, 84511 Bratislava, Slovak Republic*

[c]*Faculty of Medicine, Comenius University, Spitalska 24, 81372 Bratislava, Slovak Republic*

[d]*Selecta Biotech SE, Istrijska 20, 84107 Bratislava, Slovak Republic*

[e]*Slovak Medical University, Limbova 12, 83303 Bratislava, Slovak Republic*

[f]*Institute of Experimental Endocrinology, Biomedical Research Center, Slovak Academy of Sciences, Dubravska Cesta 9, 84505 Bratislava, Slovak Republic*

† Electronic supplementary information (ESI) available. See DOI: 10.1039/d0ra03133j

There is a very limited amount of literature on the changes of kidney function induced by nanoparticles.[16] Recent studies have shown that nanoparticle accumulation in the kidney is mostly restricted to the glomerular mesangium owing to intensive mesangial cell uptake.[17,18] Whether or not nanoparticles can reach the podocytes depends on the health state of the kidney. Given the kidney filtration threshold of about 7 nm and the size of the majority of therapeutic nanoparticles ranging between 30–150 nm, they are generally disqualified from the filtration into the urine.[19] However, in many glomerular diseases, especially involving podocyte foot effacement, the glomerular filtration barrier is damaged and leaky for bigger particles. This concern underlines the necessity of *in vitro* studies focusing on both renal cell types to provide complex information about biological effects of nanoparticles concerning the kidney filtration function.

Iron oxide magnetite nanoparticles (MNPs) are very promising candidates of modern nanotechnology research within biomedicine providing a hope of conquering unspecificity and unwanted side effects of current lege artis therapy.[20,21] They are already used for magnetic resonance imaging as contrast agents.[22,23] The real potential of MNPs in medical applications strongly depends on their physico-chemical properties as well as their coating, since the overall surface characteristics of MNPs are considered one of the most important determinants of their biological performance.[24,25] Beside the desired therapeutical action, the interactions between cells and nanoparticles can also lead to harmful nanoparticle-cell interplay[26–28] that could be rightfully considered a fundamental problem hindering translation of nanosystems into clinical practice. Only deep understanding of the nano : bio interplay enables accurate prediction and management of potential risks within development of "safe-by-design" nanomaterials.[27]

In our study we addressed the role of magnetic nanoparticles (MNPs) coated with polyethylene glycol (MNP-SO-PEG) and bovine serum albumin (MNP-SO-BSA) in renal toxicity *in vitro* and determined their impact on two neighbouring cell types of the renal glomerulum involved in blood filtration – mesangial cells and podocytes. Renal glomeruli of SV129 mice were used for isolation of primary mouse mesangial cells and primary mouse podocytes, which represent the most crucial parts of the renal glomerular filtration unit *in vitro*.

Materials and methods

Magnetite nanoparticles and DLS measurements

Magnetite nanoparticles were prepared as previously described.[28,29] Briefly, MNPs were coated with sodium oleate and polyethylene glycol (MNP-SO-PEG, D_H = 76 nm) or sodium oleate and bovine serum albumin (MNP-SO-BSA, D_H = 70 nm). Characteristics of both types of MNPs are shown in the Table 1. These parameters including particle size distribution, hydrodynamic diameter, and zeta potential in water as well as in culture media at 37 °C were determined by dynamic light scattering using Zetasizer Nano-ZS (Malvern Instruments, UK).

Animals

Kidneys from SV129 mice (Velaz, Czech Republic) at 10–25 weeks of age were used for renal cell isolation. Animals were housed in SPF facility with 12/12 hours day/night cycle and had free access to chow and water. Kidney extraction was performed after intraperitoneal thiopental euthanasia. All animal handlings were done in accordance with The Slovak Animal Protection Act subject to The European Union legislation on animal welfare EU Directive 2010/63/EU for animal experiments and were approved by The State Veterinary and Food Administration of the Slovak Republic under the approval numbers 2159/17-221 and 1638/18-221/3.

Cell culture and stimulation

Mouse glomeruli were isolated with a technique using spherical magnetic beads which allows the isolation of virtually all glomeruli present in the mouse kidney at the purity of 97%.[30] In brief (ESI S1†), transcardiac perfusion of HBSS medium (Invitrogen) containing 8×10^7 inactivated Dynabeads (Dynabeads M450 tosylactivated, Dynal) was performed to enrich Dynabeads in kidney glomeruli. Kidneys were then minced into 1 mm^3 pieces and digested with 1 mg mL^{-1} collagenase A (Calbiochem) at 37 °C for 30 minutes. After being gently pressed through a 100 μm cell strainer twice, the cell suspension was centrifuged at 200 × *g* for 5 minutes. Cell pellet was resuspended in 5 mL of HBSS and glomeruli containing Dynabeads were gathered using magnetic particle concentrator. Following washing with HBSS, glomeruli were cultured in cell-specific media. For culturing primary podocytes out of glomeruli, 1640 RPMI medium with GlutaMAX (Gibco) has been used, supplemented with 10% heat inactivated fetal calf serum (FCS, Gibco) 100 U mL^{-1} penicillin and 10 mg mL^{-1} streptomycin, 5 mmol L^{-1} HEPES (Sigma-Aldrich), 1 g L^{-1} nonessential amino-acids, 1 mmol L^{-1} sodium pyruvate (all PAA, GE Healthcare), 10 mg L^{-1} insulin-transferring-sodium-selenite supplement (Gibco). Primary mesangial cells from glomeruli were grown in high glucose (4500 mg L^{-1} glucose) DMEM (Dulbecco's Modified Eagle's medium, Gibco), supplemented with 10% heat inactivated FCS (Gibco), 100 U mL^{-1} penicillin and 10 mg mL^{-1} streptomycin, and 10 mg L^{-1} insulin-transferring-sodium-selenite supplement (Gibco). Cells were cultured in 37 °C with 5% CO_2. For experiments, cells were kept in serum free medium for 24 hours and then exposed to nanoparticles for 5 and 24 hours in medium containing 2% FCS.

Cell growth

Primary podocytes and mesangial cells were seeded onto 24-well plates (3×10^4 cells per well) and were incubated with various concentrations of MNP-SO-PEG and MNP-SO-BSA. Cells were monitored with IncuCyte™ ZOOM Live-Cell Analysis system (Essen Instruments, Ann Arbor, MI) and growth curves were constructed from calculation of cell density measurements acquired during round-the-clock kinetic imaging for 48 hours from each imaging field. All experiments were performed in triplicates and data are expressed as means ± SEM. A general

Table 1 Characteristics of surface-modified MNPs nanospheres in deionized water and in culture media

	Characteristics							
	In deionized water		In media					
Particles	Size (nm)	ζ (mV)	Medium	Concentration (mM)	d_{mean} (nm)	PDI	Stable (24 h)	ζ (mV)
MNP-SO-PEG	76 ± 1.53	−42.3	DMEM	0.1	243 ± 7	0.159 ± 0.009	Yes	−15.8 ± 0.9
				0.05	241 ± 6	0.157 ± 0.017		−16.0 ± 1.0
			RPMI	0.1	258 ± 19	0.168 ± 0.007	Yes	−15.6 ± 1.2
				0.05	255 ± 18	0.171 ± 0.006		−16.1 ± 0.9
MNP-SO-BSA	70 ± 1.29	−37.2	DMEM	0.1	97 ± 8	0.137 ± 0.013	Yes	−16.3 ± 1.0
				0.05	101 ± 10	0.134 ± 0.015		−16.7 ± 0.8
			RPMI	0.1	84 ± 9	0.138 ± 0.012	Yes	−15.4 ± 0.9
				0.05	86 ± 6	0.137 ± 0.013		−15.8 ± 1.1

linear model (GLM) for repeated measures was used for the analysis of differences in the cell growth between individual MNPs concentrations. The effects of dose and dose–time interactions were assessed.

Cytotoxicity assay

Cytotoxicity was assessed using the MTT colorimetric assay as described before.[28] Podocytes and mesangial cells (5×10^4 cells per well) were seeded onto a 96 well-plate and incubated for 24 hours with indicated concentrations of MNP-SO-PEG and MNP-SO-BSA. After removal of medium and washing with PBS, 150 μL of MTT reagent (1 mg mL^{-1}) was added to each well and incubated at 37 °C for 4 hours. Finally, 100 μL of DMSO was added and cells were agitated for 30 minutes at room temperature. Absorbance was measured at 540 nm on ELISA reader (X-mark, Bio-Rad).

Immunocytochemistry

Primary mouse podocytes and mesangial cells (4×10^4 cells) were seeded on circular cover glasses (10 mm diameter). After exposure to nanoparticles, cells were washed with PBS and fixed with 4% PFA for 15 minutes. After incubation with a specific antibody Phalloidin Alexa Fluor 546 conjugated (Life Technologies) and/or anti-vinculin (Abcam) the cell nuclei were counterstained with DAPI. The cell actin cytoskeleton was analyzed using Metafer fluorescence microscope (MetaSystems, Alogo, Ltd., Czech Republic) using Zeiss Axio Imager.Z2 and evaluated by the ISIS software. Cell area measurements were done from phalloidin-labelled cell outlines detected and analyzed using ImageJ software.

qRT-PCR

Total RNA was isolated with TRI reagent (Sigma-Aldrich) and treated with RNase-free DNase I (Thermo Scientific™) to remove genomic DNA. 0.5 μg of total RNA was used for cDNA synthesis using RevertAid First Strand cDNA Synthesis Kit (Thermo Scientific™). Semi-quantitative real-time PCR was performed using SYBR Green Real-time PCR Master Mix (Thermo Scientific™) in a CFX96 real-time PCR cycler (Bio-Rad). Primer sequences used were as follows: *Tnf-α* forward 5′-CCCACGTCGTAGCAAACCACCAAG-3′ and reverse primer 5′-TCCAAAGTAGACCTGCCCGGACTC-3′; *Il-6* forward 5′-CCAGTTGCCTTCTTGGGACTGATG-3′ and reverse primer 5′-CCTCCGACTTGTGAAGTGGTATAG-3′; *Mip2* forward 5′-GCTTCCTCGGGCACTCCAGAC-3′ and reverse primer 5′-TTAGCCTTGCCTTTGTTCAGTAT-3′;[31] *iNos* forward 5′-GCTCGCTTTGCCACGGACGA-3′ and reverse primer 5′-AAGG-CAGCGGGCACATGCAA-3′; *α-Sma* forward 5′-CACCATGTACC-CAGGCATTG-3′ and reverse primer 5′-GGCCCAGCTTCGTCGTATTC-3′; fibronectin forward 5′-ATG-CACCGATTGTCAACAGA-3′ and reverse primer 5′-TGCCGCAACTACTGTGATTC-3′; collagen III forward 5′-TGGTTTCTTCTCACCCTTCTTC-3′ and reverse primer 5′-TGCATCCAAATTCATCTACGT-3′; *Epcam* forward 5′-CATTTGCTCCAAACTGGCGT-3′ and reverse primer 5′-TGTCCTTGTCGGTTCTTCGG-3′; *Wt-1* forward 5′-TCTTCCGAGGCATTCAGGAT-3′ and reverse primer 5′-TGCTGACCGGACAAGAGTTG-3′; nephrin forward 5′-GCAT-CACTCTGCAGGTCACCTTTC-3′ and reverse primer 5′-AGGC-CATCCATGACTGTCTCATCC-3′; podocin forward 5′-AAGTGCGGGTGATTGCTGCAGAAG-3′ and reverse primer 5′-TGTGGACAGCGACTGAAGAGTGTG-3′; and *Polr2a* forward 5′-CTCGAAACCAGGATGATCTGACTC-3′ and reverse primer 5′-CACACCCACTTGGTCAATGGATAG-3′, which was used as housekeeping gene. Relative expression levels of target genes were normalized to *Polr2a* and calculated by the $2^{-\Delta\Delta C_T}$ method and are given as exposed to control samples ratio. All experiments were performed in triplicate. Data are expressed as means ± SEM.

Western blotting

Cell lysates were prepared using RIPA cell lysis buffer containing 50 mM Tris HCl, pH 7.4, 150 mM NaCl, 1% Triton X-100, 0.5% sodium deoxylcholate, 0.1% SDS, supplemented with the cOmplete™, Mini Protease Inhibitor Cocktail (Sigma-Aldrich, Lambda Life, Ltd., Slovakia) and phosphatase inhibitor cocktail PhosSTOP™ (Sigma-Aldrich, Lambda Life, Ltd., Slovakia). Protein concentration was determined using the Bradford assay. Equal amounts of proteins were boiled in Laemmli buffer, separated on 10% SDS-PAGE gel and transferred to a nitrocellulose membrane (Amersham, Prosciencetech, Ltd.,

Slovakia). After blocking, the membranes were incubated at 4 °C overnight with the following primary antibodies: GAPDH (Cell Signaling Technology), and iNOS (Enzo Life Sciences). Secondary goat anti-mouse- or goat anti-rabbit-IR-Dye 680 or 790 antibodies (Invitrogen) were visualized by an Odyssey Imaging System (LI-COR Biosciences) and densitometry was evaluated with the Odyssey package. All experiments were performed in triplicate. Results were normalized to GAPDH content and data are given as mean ± SEM.

Transmission electron microscopy (TEM)

Podocyte and mesangial cell suspension was centrifugated at 1000 × g_{max} for 10 min in 2% glutaraldehyde in cacodylate buffer (150 mM Na-cacodylate, 2.0 mM $CaCl_2$; pH 7.3). Pelleted cells were further fixed with 2% glutaraldehyde in cacodylate buffer for 3.5 hours. Subsequently, the samples were post-fixed with 1% osmium tetroxide in cacodylate buffer for 45 min at room temperature and stained with 1% aqueous uranyl acetate. After dehydration in a graded ethanol series and propylene oxide, the samples were embedded in Durcupan (Fluka). Ultrathin (58–60 nm) sections were cut with a Power-Tome MT-XL (RMC/Sorvall, USA) ultramicrotome, placed on copper grids covered with Formvar and stained with lead citrate. The sections were examined with a JEM 1200 electron microscope (Jeol, Japan). Images were recorded using a Gatan Dual Vision 300W CCD camera (Gatan, USA).

Atomic absorption spectrometry (AAS)

The uptake of MNP-SO-PEG and MNP-SO-BSA by podocytes and mesangial cells was quantified by AAS. Analyses were carried out by flame AAS for iron (Fe). Cell pellet was digested with 500 μL 65% HNO_3 in ultrasonic bath at 85 °C for 5 hours and diluted with 2% HNO_3 in deionized water. Iron content in the samples has been estimated using the following instrumental parameters: wavelength 248.3 nm, slit width 0.2 nm, flame type: acetylene-air, flow: 2.0 L min^{-1} for acetylene and 13.5 L min^{-1} for air, deuterium background correction, method of calibration curve in the range 0.1–10 mg mL^{-1}. The limit of detection and the limit of quantification were set to 0.002 mg L^{-1} and 0.025 mg L^{-1} for AAS, respectively.

Statistical analysis

Data were analyzed by paired or unpaired *t* test or analyses of variance (ANOVA), with and without repeated measurements, followed by Fisher's LSD post hoc test, depending on the experimental design, as well as by a general linear model (GLM) for repeated measures. The normality of distribution was assessed by Shapiro–Wilk tests. If normally distributed, sample means were tested by the analysis of variance (ANOVA) with the Bonferroni's or Tamhane's corrections, depending on the homogeneity of variance. For non-normally distributed data the Dunn or Dunn–Bonferroni *post hoc* method was applied following a significant Kruskal–Wallis test. IBM SPSS statistics version 23.0 software for Windows (IBM) was used for statistical analyses of the data. Results are given as means ± SEM. Differences were considered significant at a P value of <0.05.

Results

Basic characteristics of MNPs in the solvent and biological environment

Physico-chemical properties of nanoparticles estimated in the solvent may be altered in biological environment. Therefore, the basic characteristics of surface modified MNPs (particle size, colloidal stability, zeta-potential and particle size distribution) were analyzed both in the solvent as well as in the culture media. All these parameters are shown in the Table 1. In RPMI medium, size of magnetite nanoparticles coated with PEG (MNP-SO-PEG) increased almost 4 times and zeta-potential decreased by about 50% compared to the data measured in water. Parameters obtained in DMEM were very similar. Interestingly, size of magnetite nanoparticles coated with BSA (MNP-SO-BSA) has changed only minimally in the tested media compared to water while zeta-potential lowered about a half. Colloidal stability of both MNPs in biologically relevant media remained unaltered within 24 hours what allowed us to reliably investigate the induced biological effects up to 24 hours time points (Table 1) without additional effects that would bias the obtained results. It is evident already from this data that MNP-SO-PEG and MNP-SO-BSA behave differently in the biological environment, though, it is to be expected that their biological activity would also be different.

The impact of surface modified MNPs on renal cell viability and proliferation activity

To investigate the cytotoxicity of surface modified MNPs and their impact on cell viability we performed cell culture experiments in murine renal cells. Both primary renal mesangial cells and podocytes were isolated directly from mouse kidney to obtain the *in vitro* model most representative to the *in vivo* situation (ESI S1†). Podocytes and mesangial cells were let grown from isolated mouse glomeruli (Fig. 1B) in cell type-specific media. Purity of the cultured primary podocytes has been verified by analysis of podocyte-specific markers *Wt-1*, nephrin, and podocin (Fig. 1A). Complete lack of podocyte markers in the supernatant fraction representing the tubular part of the kidney indicated high purity of glomeruli isolation. As expected, we observed dedifferentiation of podocytes under *in vitro* culture conditions, especially a decrease in expression of podocyte slit diaphragm proteins nephrin and podocin (Fig. 1A), as well as an increase in expression levels of mesenchymal markers fibronectin and *α-Sma* with the number of passages (Fig. 1C). Expression of *Epcam*, an epithelial cell adhesion molecule considered a marker of epithelial cells decreased already with the second passage of podocytes (Fig. 1D). It is of note that *Epcam* level was very high in the supernatant fraction due to the presence of tubular epithelial cells (Fig. 1D). Despite this, primary podocytes still represent the best model for *in vitro* studying of podocyte responses towards different stimuli. On the other hand, mesangial cells synthesized about 5-times more collagen III than podocytes (Fig. 1E) and did not express podocyte markers (Fig. 1E). These two very distinct renal cell types, concerning their structure as

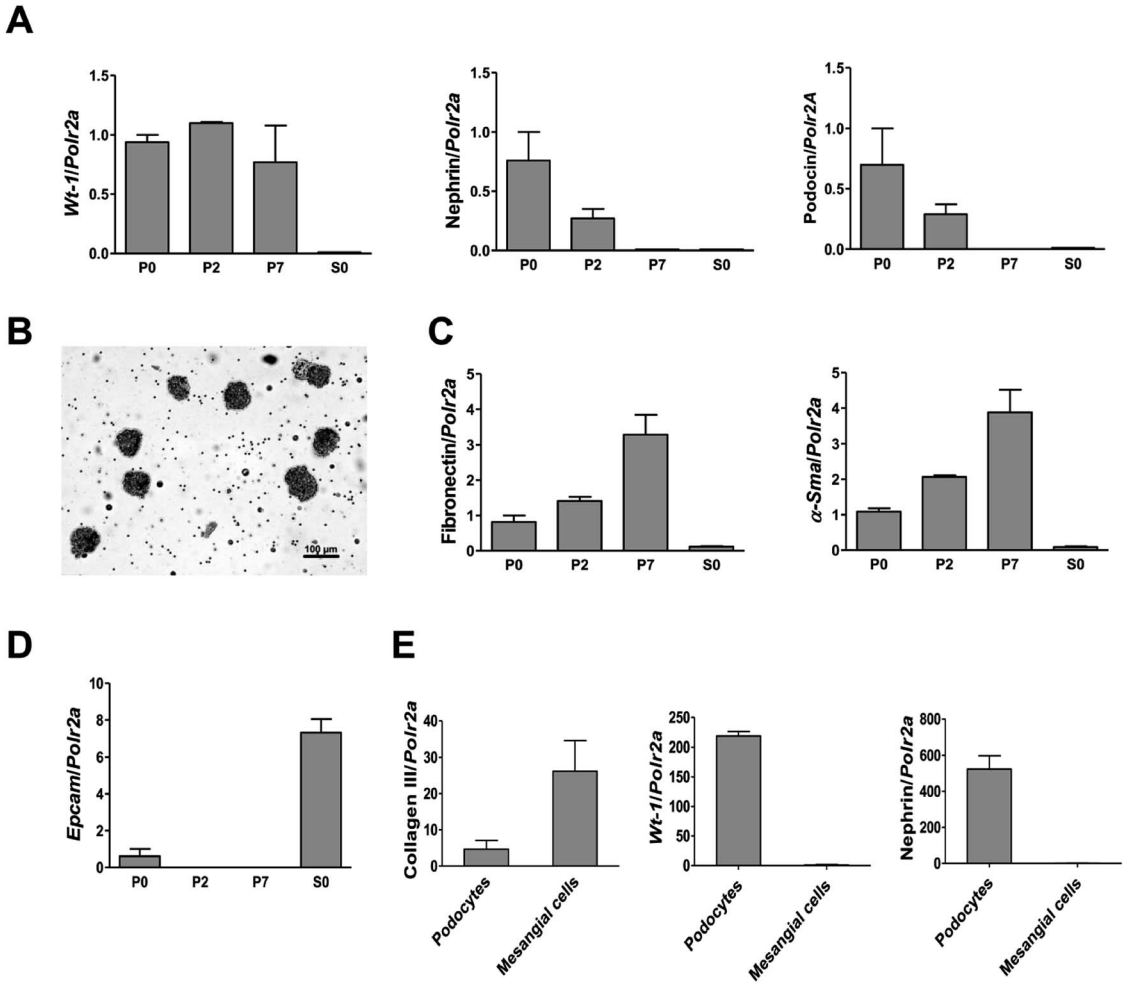

Fig. 1 Characterization of primary cultures of podocytes and mesangial cells isolated from mouse glomeruli. RT-PCR analysis of the podocyte specific markers *Wt-1*, nephrin, and podocin expression in primary podocytes (A). Representative image (scale bar 100 μm) of glomeruli after isolation with Dynabeads (B). Expression of fibronectin, smooth muscle α-actin (*α-Sma*) (C), and epithelial cell adhesion molecule (*Epcam*) (D) in primary podocyte culture. Comparison of collagen III, *Wt-1*, and nephrin expressions between primary cell cultures of podocytes and mesangial cells after the second passage (E). Data represent the mean ± SEM of three independent experiments. P0: primary podocytes grown out from glomeruli before passaging. P2: primary podocytes after two passages. P7: primary podocytes after seven passages. S0: supernatant fraction (=tubular part of nephrons after isolation).

well as function, represented the basis for the following *in vitro* study of MNPs-induced effects in the renal tissue. Cytotoxicity of both types MNPs was evaluated after 24 h treatment. While MNP-SO-PEG were highly toxic for podocytes at a concentration of 0.3 mM, no decrease in cell viability was determined for mesangial cells (Fig. 2A).

On the other hand, MNP-SO-BSA were toxic for both mesangial cells and podocytes at given concentrations (Fig. 2B). These results show that podocytes are more susceptible to MNPs than mesangial cells. Differences in toxicity between MNP-SO-PEG and MNP-SO-BSA indicate that the coating plays an important role in the cytotoxicity of MNPs. To study the proliferation activity of exposed cells in more details, the cell growth was analyzed using IncuCyte system. Both podocytes and mesangial cells were exposed to non, low as well as highly toxic concentrations of MNPs for 48 h. MNP-SO-PEG caused dose-dependent growth reduction in podocytes, however, none of the tested concentrations affected the growth of mesangial cells (Fig. 2C). MNP-SO-BSA affected the growth of both podocytes and mesangial cells only at the highest concentration (Fig. 2D). These results demonstrate that one type of MNPs may induce diverse responses in distinct cell types (mesangial cells *vs.* podocytes) even if originating from the same tissue.

MNPs induce pronounced inflammatory response in podocytes but not in mesangial cells

The capacity of MNP-SO-PEG and MNP-SO-BSA to induce inflammation in podocytes and mesangial cells was investigated at non-/low-toxic concentration range (0.01–0.07 mM) after short-term (5 h) and long-term exposure (24 h). In podocytes, MNP-SO-PEG-induced mRNA expression of proinflammatory factors *Tnfα*, *Il-6*, *Mip2*, and *iNos* was detected at 5 h time point (Fig. 3A).

However, this response became much more pronounced after 24 hours of exposure (Fig. 3A). Increase in TNFα and IL-6

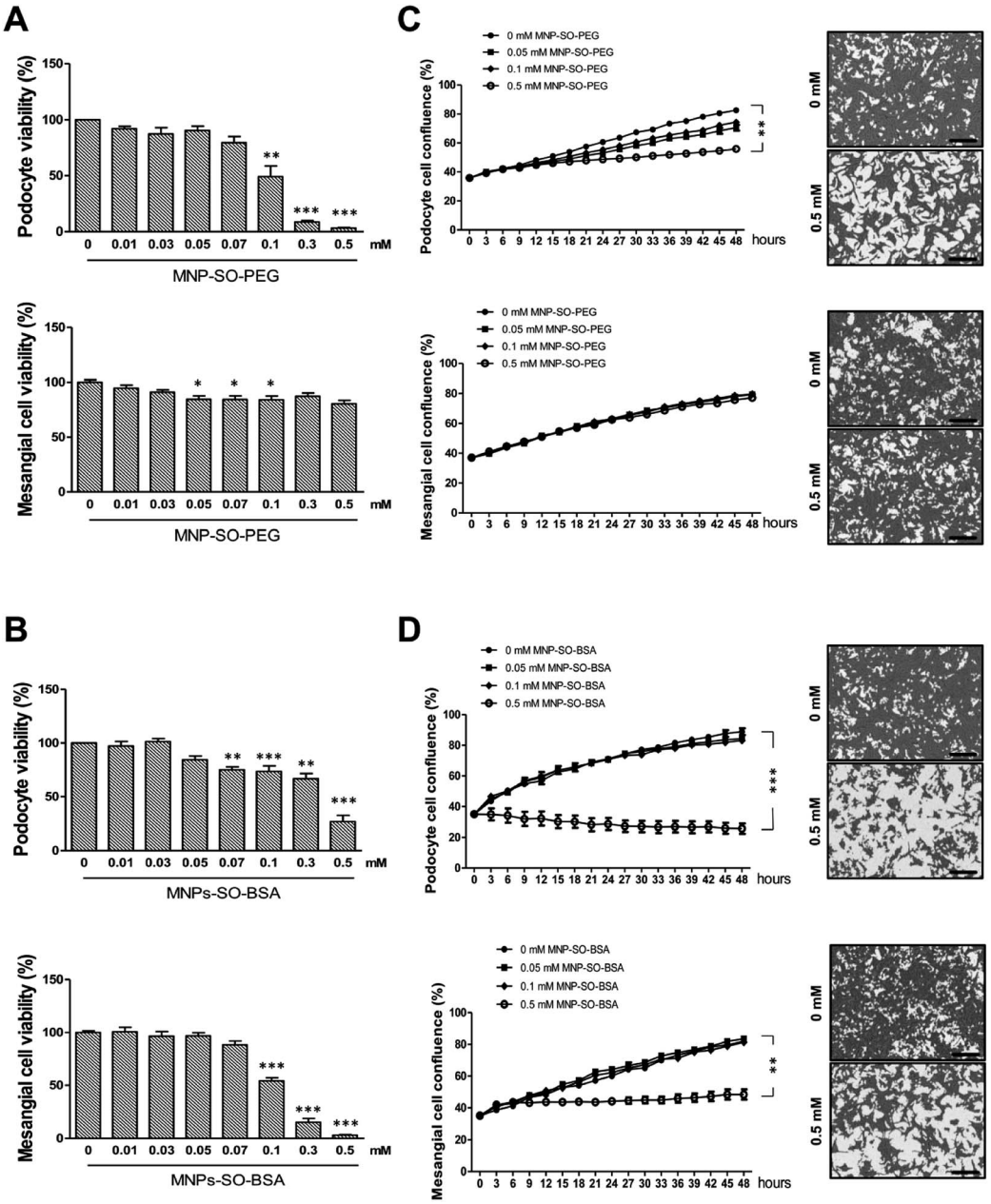

Fig. 2 MNPs exert different cytotoxic profiles on primary podocytes and mesangial cells. Cytotoxicity of MNPs on primary podocytes and mesangial cells determined by MTT assay for MNP-SO-PEG (A) and MNP-SO-BSA (B) shown as percentage of viable cells after 24 h exposure with indicated extracellular concentrations of nanoparticles. Real-time analysis of growth of primary podocytes and mesangial cells under influence of MNP-SO-PEG (C) and MNP-SO-BSA (D) in indicated extracellular concentrations of nanoparticles using IncuCyte ZOOM Imager for 48 h monitoring. Right panel images show confluency masking and measurement in cells from corresponding graph measurement in the absence (0 mM) and presence (0.5 mM) of MNPs. Scale bar represents 300 μm. The data are representative of three independent experiments and are means ± SEM. $*P < 0.05$, $**P < 0.01$, and $***P < 0.001$ *vs.* corresponding non-exposed control.

secreted protein levels were also confirmed after 24 h of stimulation by MNP-SO-PEG (Fig. 4A), as well as elevation of newly synthesized iNOS protein (Fig. 4B). In mesangial cells, inflammatory response to MNP-SO-PEG was very modest compared to podocytes. Only very small induction of *Tnfα* and *Il-6* was detected after 5 h with none of the inflammatory factors elevated at 24 h time point except for *iNos* (Fig. 3A). These findings were confirmed on the protein level as well (Fig. 4A and B). MNP-SO-BSA caused moderate induction of *Il-6*, *Mip2*, and *iNos* after 5 h in podocytes, but expression levels of all proinflammatory factors were low after 24 h (Fig. 3B). There was no increase in cytokines or iNOS at the protein level detected after 24 h (Fig. 4A and C). This is in a strong contrast with high expression levels of these factors after 24 h in case of MNP-SO-PEG. In mesangial cells, except for the increase in *Tnfα*, expression of proinflammatory factors remained low in the

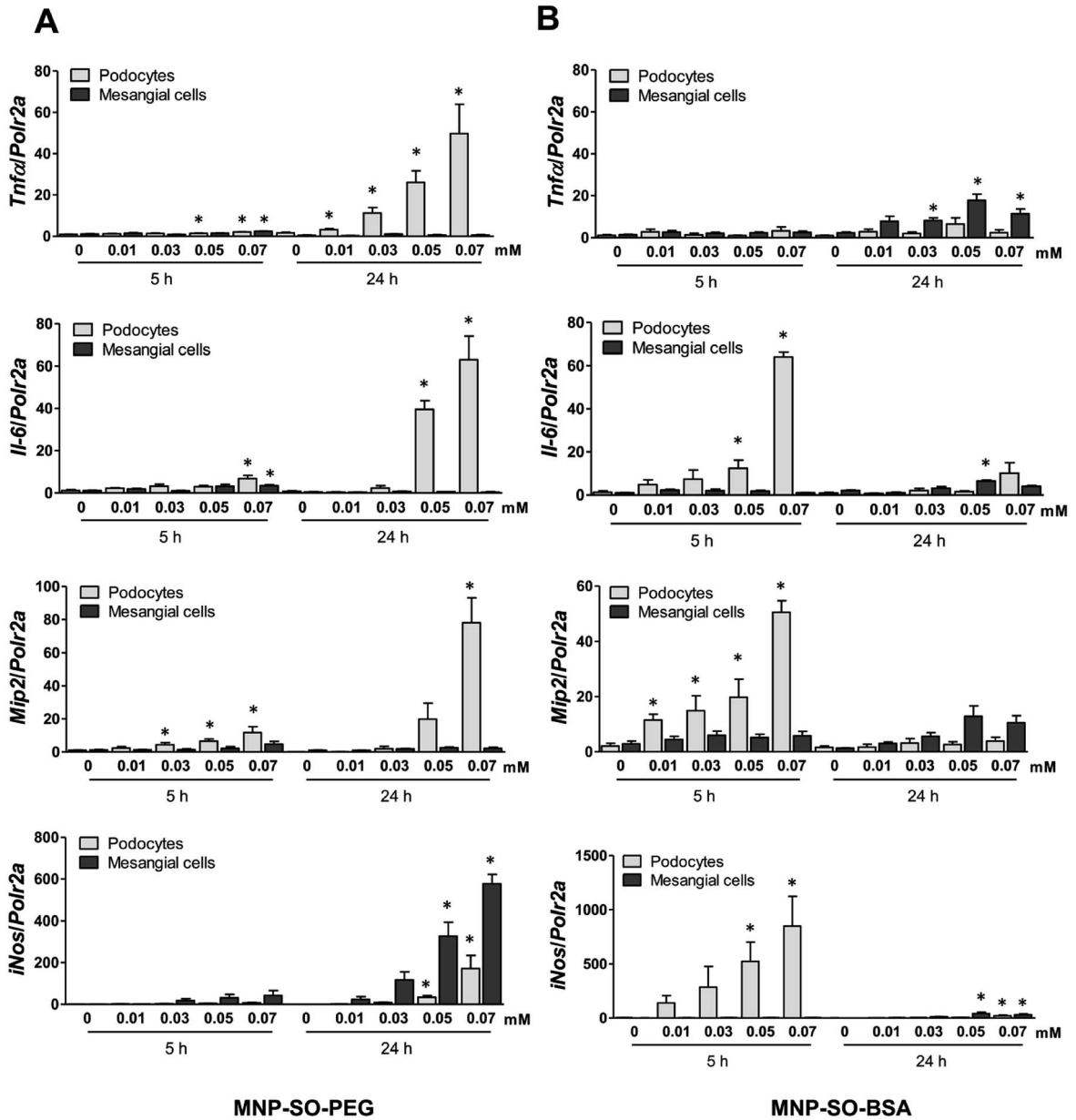

Fig. 3 MNPs induce more intensive inflammatory response in murine podocytes than in mesangial cells. RT-PCR for *Tnfα*, *Il-6*, *Mip2*, and *iNos* after the short (5 h) and long (24 h) time exposure to indicated concentrations of MNP-SO-PEG (A) and MNP-SO-BSA (B). Data represent the mean ± SEM of three independent experiments. $*P < 0.05$ *vs.* corresponding non-exposed control.

presence of MNP-SO-BSA (Fig. 3B) which was confirmed also at the protein level (Fig. 4A and C).

Actin cytoskeleton changes of podocytes and mesangial cells correspond to amount of internalized MNPs

Podocyte foot processes and slit diaphragm are pivotal components of the glomerular filter, and disruption of their integrity is a critical event in the development of proteinuria and nephrotic syndrome in a variety of inherited and acquired glomerular disorders.[14,32,33] Therefore, cell cytoskeleton changes in podocytes upon MNPs uptake were examined. MNP-SO-PEG as well as MNP-SO-BSA caused rearrangement of podocyte actin cytoskeleton in a dose dependent manner (Fig. 5A and B) and this was associated with reduction of adhesive properties of podocytes (Fig. 5C). MNPs-mediated impact on podocyte cell shape was confirmed also by the cell area reduction (Fig. 6A). Much moderate changes were observed in mesangial cells upon exposure to both types of MNPs (Fig. 5A–C and 6A). Importantly, the potential of MNPs to damage podocyte structure and impair their adhesion is the most detrimental of all MNPs-induced effects possibly leading to definitive podocyte loss in case of MNPs uptake. Interestingly, severity of changes in cytoskeletal organization corresponded to the amount of MNPs internalized by each cell type. As shown by atomic absorption spectroscopy (AAS) the amount of internalized MNPs differed dramatically between podocytes and mesangial cells. Stunningly, podocytes

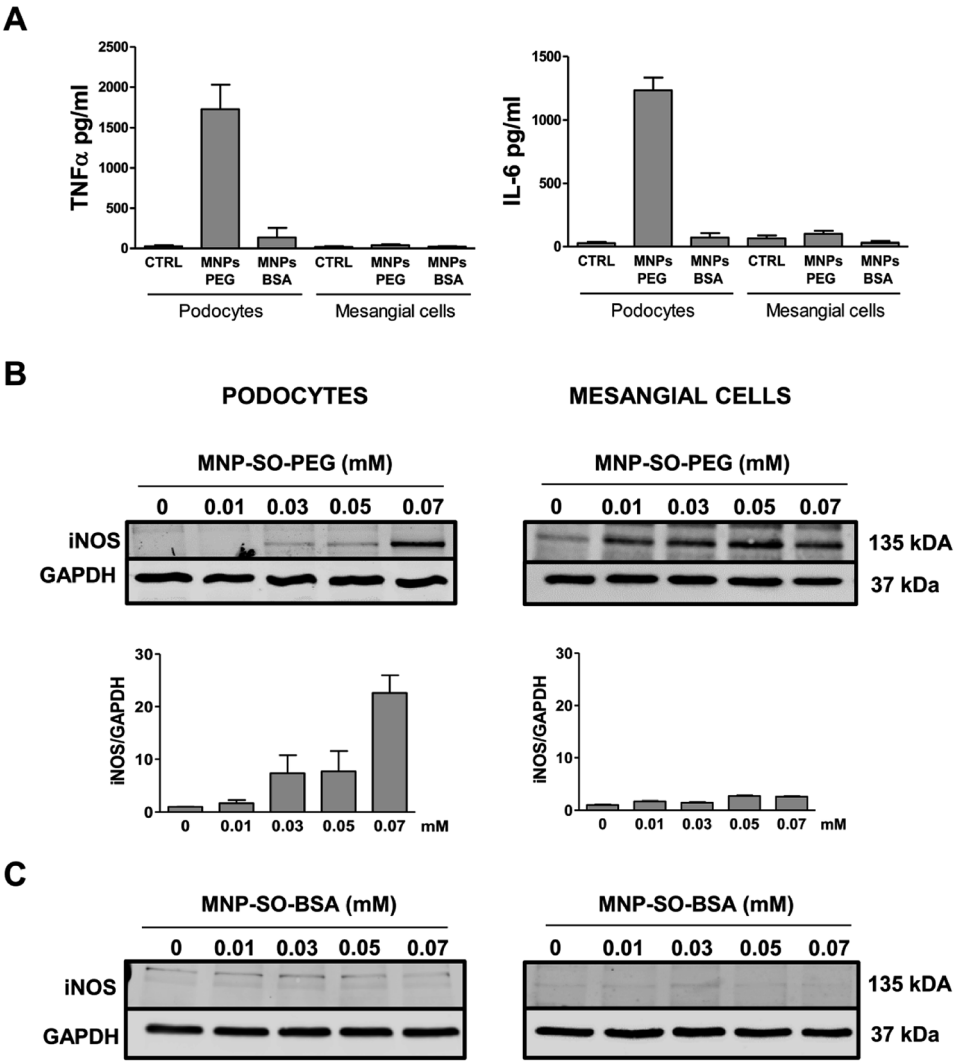

Fig. 4 Inflammatory protein synthesis is triggered more by MNP-SO-PEG than MNP-SO-BSA. Cytokine secretion determined by ELISA for TNFα and IL-6 in cell culture supernatants from primary podocytes and mesangial cells after 24 h exposure to MNP-SO-PEG and MNP-SO-BSA (A). Western blots for iNOS produced by primary podocytes and mesangial cells incubated with or without indicated concentrations of MNP-SO-PEG and their quantification (B) and MNP-SO-BSA (C). MNPs PEG: MNP-SO-PEG, MNPs BSA: MNP-SO-BSA. Data represent the mean ± SEM of three independent experiments.

were able to internalize about 5–6 times more nanoparticles than mesangial cells at equimolar concentration after 24 h treatment (Fig. 6B).

Ultrastructural characteristics of mesangial cells and podocyptes after internalization of magnetic nanoparticles

The electron microscopy analysis confirmed presence of both types of MNPs in mesangial cells as well as in podocytes (Fig. 7 and 8) and revealed that nanoparticles entered the cells by phagocytosis (Fig. 7A) eventually accumulating in lysosomes (Fig. 7 and 8) in both cell types. Uptake of MNP-SO-BSA led to formation of phagolysosomes (Fig. 7B and C) and autophagic vacuoles containing MNPs and myelin-like structures that were localized mainly under the plasma membrane and in the perinuclear zone (Fig. 7D). From the total cell population, as much as 70% of mesangial cells contained phagolysosomes with MNP-SO-BSA, whereas in podocytes, they were present in 80% of the cells, estimated by visual appraisal. Compared to mesangial cells, podocytes containing internalized MNP-SO-BSA often displayed significant swelling of cisterns of Golgi complex (Fig. 7C). On the other hand, exposure of cells to MNP-SO-PEG led to formation of extensive vacuoles containing degraded organelles and nanoparticles in both cell types (Fig. 8A and B). Cytosol of cells was rich in nanoparticle-containing phagolysosomes (Fig. 8C and D), fragments of endoplasmic reticulum (Fig. 8C), and mitochondria often displaying signs of damage (Fig. 8C and D).

Discussion

In this study we evaluated the impact of MNPs on two types of renal glomerular cells isolated from mouse kidneys – podocytes

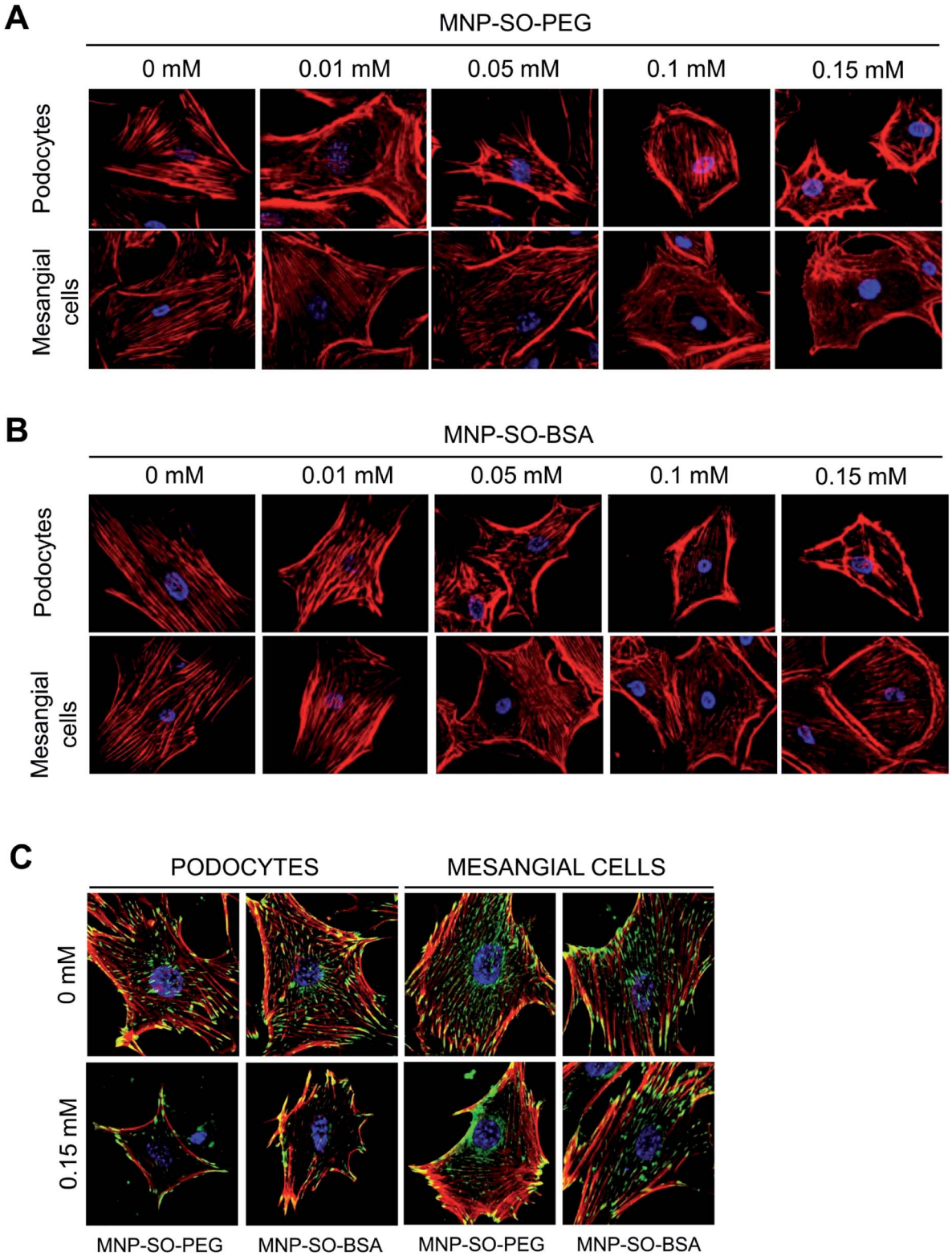

Fig. 5 MNPs-induced cellular responses involve concentration dependent remodeling of actin cytoskeleton. Phalloidin staining of the actin cytoskeleton in podocytes and mesangial cells after 24 h incubation with or without indicated concentrations of MNP-SO-PEG (A) or MNP-SO-BSA (B). Red – phalloidin, blue – DAPI. Magnification 630×. MNPs cause reduction of adhesive properties of podocytes and to a lesser extent of mesangial cells. Staining of focal adhesion molecule vinculin after 24 h incubation with or without 0.15 mM MNP-SO-PEG or MNP-SO-BSA (C). Red – phalloidin, green – vinculin, blue – DAPI. Magnification 630×.

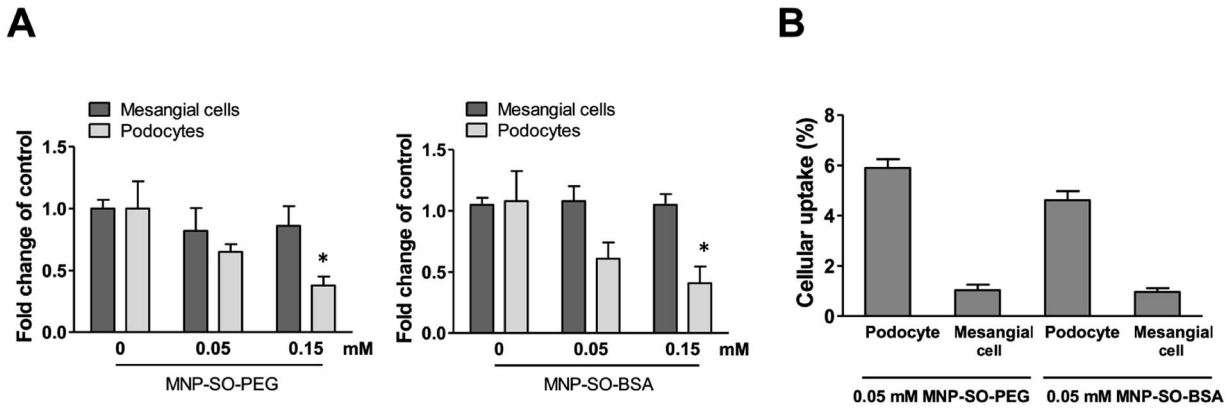

Fig. 6 MNPs cause reduction in cell area of podocytes but not mesangial cells. Cell area calculated from fluorescent images of mesangial cells and podocytes after 24 h exposure to MNP-SO-PEG and MNP-SO-BSA (A). Data represent the mean ± SEM of three independent experiments. *$P < 0.05$ *vs.* corresponding non-exposed control. Uptake of MNPs by podocytes and mesangial cells (4×10^5 cells) after 24 h exposure to 0.05 mM MNP-SO-PEG and 0.05 mM MNP-SO-BSA expressed as percentage of pg Fe internalized per cell/pg Fe available per cell (B). The data are representative of three independent experiments and are means ± SEM.

and mesangial cells. Despite originating from the same glomeruli and being in close proximity within the glomerular structure, podocytes and mesangial cells displayed vastly different responses to MNPs. MNPs coated with PEG or BSA induced expression of proinflammatory mediators such as TNFα, IL-6, iNOS, and MIP2 in cultured podocytes, while mesangial cell response was rather moderate. Ability of podocytes to internalize more fold MNPs than mesangial cells was identified as important factor underlying increased sensitivity toward nanoparticles. Primary cell cultures were used to obtain the data that are more relevant and reflective of the *in vivo* environment than those derived from studies involving stable cell lines. Recently, renewed interest in primary cells has been noted due to factors such as misidentified and

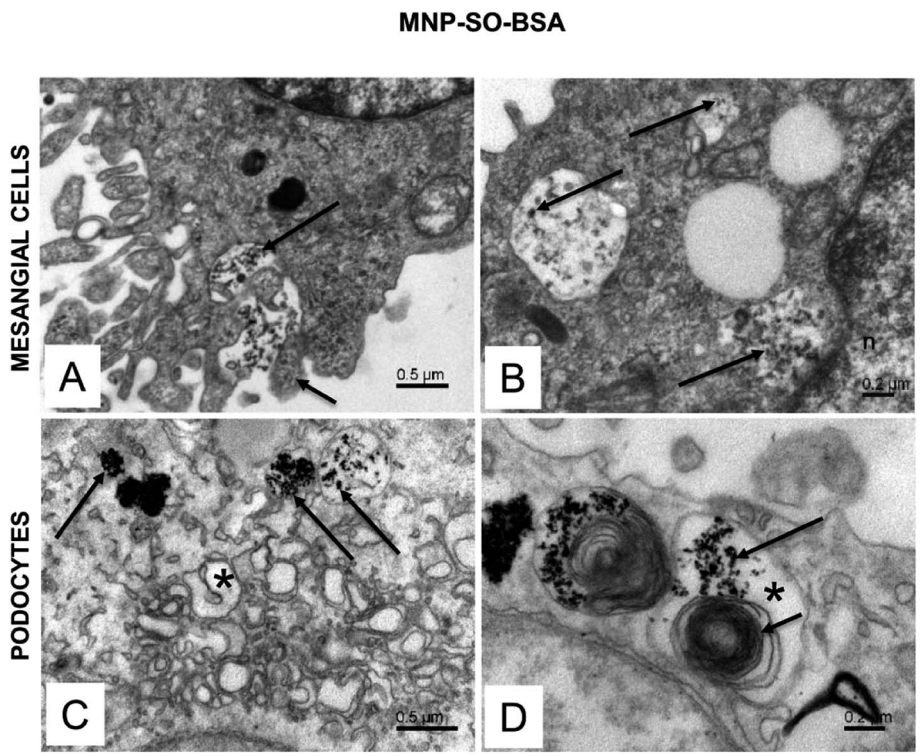

Fig. 7 Ultrastructure of mesangial cells and podocytes exposed to MNP-SO-BSA. (A) Active surface of mesangial cell with MNP-SO-BSA in the extracellular space (long arrow) and protrusions of plasma membrane (short arrow) surrounding nanoparticles. (B) Phagolysosomes (arrows) in the cytosol of mesangial cell with incorporated MNP-SO-BSA. (C) Phagolysosomes (arrows) and swollen cisterns of Golgi complex (asterisk) in the cytosol of podocytes. (D) Large autophagic vacuole (asterisk) in podocytes containing MNP-SO-BSA (long arrow) and myelin-like structures (short arrow).

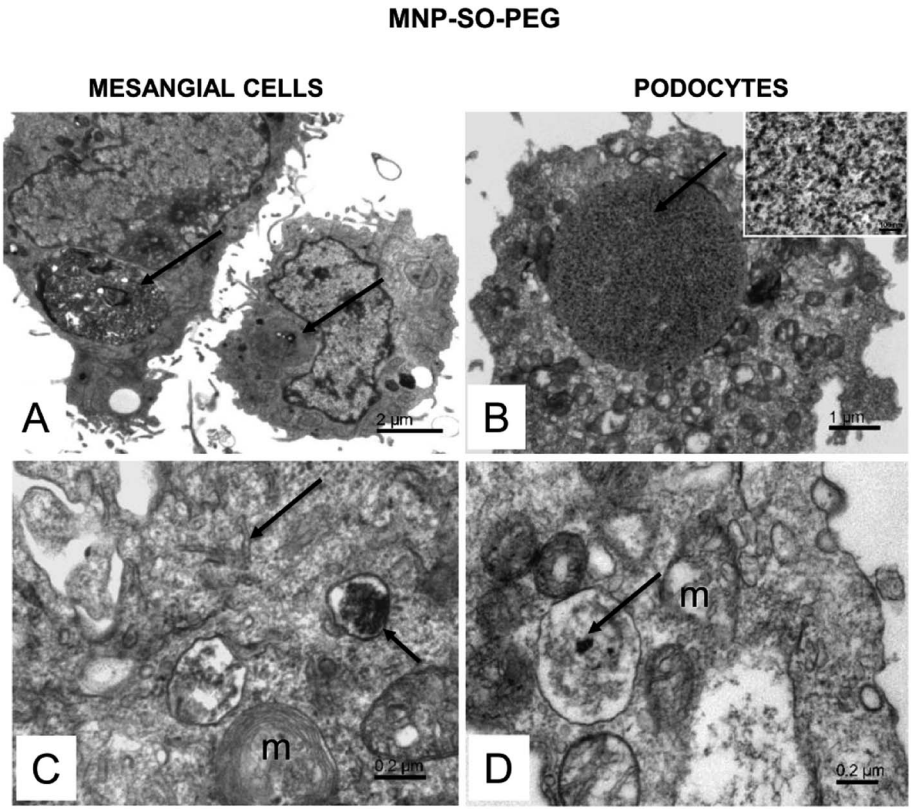

Fig. 8 Ultrastructure of mesangial cells and podocytes exposed to MNP-SO-PEG. (A) Overview of mesangial cells with large vacuoles in cytosol (arrows). (B) Podocyte with an extensive vacuole in the cytosol (arrow). The inset shows a detail of the vacuole content at large magnification. The calibration bar indicates 100 nm. The size of the granular material corresponds to MNP particles (arrow). (C) Phagolysosome (small arrow) with a dense content in the mesangial cell cytosol and fragmented endoplasmic reticulum network (arrow); m – damaged mitochondria. (D) MNPs-containing phagolysosome (arrow) in the podocyte cytosol; m – mitochondria show signs of damage.

contaminated cell lines.[34,35] Furthermore, primary cells isolated directly from tissues retain normal cell morphology and maintain many of the important markers and functions seen *in vivo*.[36,37] Even though MNPs have been in the research focus over the last years, not much is known about their impact on kidney function. At the same time, kidney is one of the target organs for nanoparticle accumulation[38,39] and renal excretion route is one of the major ways for eliminating nanoparticles as therapeutic agents from the body.[40] However, despite a great number of studies, limited information is available on MNPs-induced effects on kidney function so far. Current strategies in nanomedicine focus on the development of biocompatible nanomaterials with negligible or no toxicity[41] and renal cell preservation should be included. To increase the stability and biocompatibility, MNPs are coated with different organic natural and synthetic polymers. PEG, a synthetic biodegradable polymer, should avoid fast clearance of nanoparticles by the immune system.[42] BSA, thanks to the relatively simple modification[43] and advantageous pharmacokinetic profile owed to long blood circulation half-time,[44] became another promising coating in nanomedicine. On such a basis, we determined whether MNPs coated with PEG or BSA represent a good choice for a kidney-safe nanomaterial and we explored their impact on murine renal glomerular cells. Previous observations indicated that due to their critical role in blood filtration, renal cells are exposed to intensive toxic accumulation[17] and prolonged residency of nanoparticles has been associated with the nephrotoxicity due to excessive nanopartice uptake by these cells.[45,46] Indeed, we confirmed that mesangial cells and podocytes are able to internalize massive amount of MNPs and to store them in the specialized large lysosomes. Given that podocytes form essential barier for plasma protein loss during filtration, any damage to these cells constitute a potential risk of glomerula dysfunction. As a potential MNPs-induced undesirable impact, we focused on inflammatory response. Metal-core nanoparticles were already shown to induce inflammatory response in the cells[47,48] and contribute to inflammatory cell infiltration in the lungs of the mice.[49] Similarly, intravenous or intraarticular injection of MNPs induced acute immune responses in mice.[50] For renal cells, not much is known about MNPs-elicited inflammatory reactions, yet. Most of information regarding MNPs and kidney is provided by MRI experimental approaches using ultrasmall superparamagnetic iron oxide particles in rat or mouse models of renal failure.[51,52] However, in spite of much smaller size of these paramagnetic contrast agents compared to our MNPs, these studies rely on macrophage infiltration of the renal tissue and its detection and do not concentrate on the health-state of the renal cells *per se*. In our study, we focused on

the aspect of renal cell injury and identified MNPs as a potential trigger of inflammatory signaling. We observed that PEG-similar as BSA-coated MNPs induced expression of pro-inflammatory cytokines TNFα and IL-6 on the mRNA as well as protein level, accompanied by the expression of *Mip2* and *iNos* in podocytes. Surprisingly, the same nanoparticles did not trigger such an intensive pro-inflammatory response in mesangial cells except for *iNos*, which was strongly induced by MNP-SO-PEG. This is in agreement with the study that showed Ferucarbotran, a clinically used superparamagnetic iron oxide for magnetic resonance imaging, caused increase in mRNA expression and secretion of TNFα, IL-1β, and IL-6 cytokines in murine peritoneal macrophages that was followed by nitric oxide secretion and *iNos* mRNA synthesis.[53] To our knowledge, the present study is the first to explore inflammatory potential of MNPs in the renal cells. The conditions to detect expression of inflammatory mediators in our *in vitro* system have been adapted from the published literature. Early inflammatory cytokine release has been detected about 3 to 8 hours after stimulation and the late occurred after 24 h.[54–56] Similarly, metal-core nanoparticle-induced cytokine release in Raw 264.7 cells peaked at 24 hours after exposure.[57] Based on these data, 5 and 24 hours time-points were chosen for detection of inflammatory response in mesangial cells and podocytes exposed to MNPs. Mesangial cells responded to MNPs faintly, only MNP-SO-PEG induced synthesis of iNOS. This might be of importance considering that PEG-coated nanoparticles would accumulate with high expectancy in the glomerular mesangium and also directly in mesangial cells *in vivo*.[18] In podocytes, both types of MNPs induced inflammatory reaction, however, not by the same mechanism. Considering that the MNPs differed solely in the outer coating it is conceivable that the observed differences depend on the surface chemistry of MNPs. Indeed, the impact of MNPs coating has been suggested an important factor in toxicity of MNPs in A549 cells.[58] We observed here that MNPs with PEG, a synthetic polymer, induced cytokine activation at early time-point and this was progressively increased in the later time-point. MNPs coated with BSA, an albumin occurring naturally in the body, induced inflammatory response only at early time-point and later it was attenuated. Excitingly, it has been published earlier that endocytosis of albumin by podocytes may lead to cell death.[59] Initially, upregulation of pro-inflammatory cytokines TNFα and IL-1β mRNA with the peak at 3 hours has been detected; later a prolonged albumin exposure led to deleterious effects and has been linked to progressive podocyte loss as seen in proteinuric kidney diseases.[59] This finding is in line with our observation that MNP-SO-BSA effectively induced cytokine expression at 5 h in podocytes. Further studies should therefore be undertaken, to test whether our observation can underlie the same mechanism as albumin-mediated damage in podocytes after endocytosis. Podocytes as essential parts of the filtration barrier possess a complex structure and even minor rearrangements of actin cytoskeleton result in effacement and disappearance of podocyte actin-rich processes[60] that can result in proteinuria and glomerular damage.[61] Previously, we showed that therapeutics protecting podocyte shape are beneficial in the treatment of chronic kidney diseases.[14] In our present study, both types of MNPs initiated actin cytoskeleton rearrangement in podocytes and significant cell shrinkage was observed with higher concentrations of MNPs. This situation translated *in vivo* would mean filtration barrier breakdown. Also cytoskeleton of mesangial cells was affected by MNPs but the changes were very moderate. Dynamic assembly of actin filaments and microtubules are strictly regulated to maintain a consistent cell structure over time in differentiated cells and their rearrangement can contribute to cell damage.[62] Indeed, we previously found that MNPs can interfere with microtubules resulting in disruption of tubulin filaments in human lung A549 cells.[63] Differences between podocyte and mesangial cell sensitivity in response to MNPs are most likely to be attributed to MNPs uptake. Previously, we have shown that uptake of nanoparticles is a complex process and the amount of internalized nanoparticles depends on several factors such as number of treated cells, type of cell, type of particles, particle concentration, colloidal stability, *etc.*[64] Here we show clearly that a specific type of cell also derived from the same organ is important variable and that cell type specific nanoparticle uptake efficacy may be determining factor of cell sensitivity toward nanoparticle exposure. Previous findings indicated that poor uptake of PEGylated nanoparticles by podocytes was most probably responsible for the weak effects observed.[65] Similar correlation was found between cytotoxic effects and internalized amount of MNPs in A549 cells.[28,29] However, to our best knowledge, this is the first time that cellular uptake of nanoparticles by podocytes and mesangial cells was quantified. Podocytes internalized 6 times more MNP-SO-PEG and 4 times more MNP-SO-BSA than mesangial cells, keeping all other variables constant – cell number, nanoparticle type, experimental conditions, *etc.* This observation is very important, as it opens the debate about safety of MNPs for the patients with proteinuric kidney diseases where due to "leaky" glomerular barrier also MNPs larger than size limit for filtration can be filtered and directly reach podocyte layer. Recently, it has been suggested by others that different types of cells exhibit specific response to nanoparticles comparing human lung carcinoma and mouse fibroblast cell lines[66] or human lung epithelial cells and human monocytes[67] but none of the study focused on different types of cells residing in the same organ and possessing specific diverse functions within the organ. Another aspect concerning nanoparticle uptake was evidenced by electron microscopy analysis. TEM images of podocytes and mesangial cells revealed that the uptake of MNPs is an active process and involves phagocytosis, although other active nanoparticle uptake routs of endocytosis are not excluded. Podocytes internalized MNPs more actively than mesangial cells. This led in case of MNP-SO-BSA to a swelling response of Golgi apparatus of podocytes but not mesangial cells. Functional link between Golgi cisternae and actin filaments has already been proposed and actin depolymerization-induced cisternae swelling indicated high sensitivity of the Golgi shape to changes in the organization of the actin cytoskeleton.[68] Indeed, our immunocytochemical analysis showed that assembly of actin cytoskeleton of podocytes after exposure to MNP-SO-BSA was strongly disturbed compared to better

preserved structure of mesangial cells. Observed alteration in the architecture of the Golgi complex has also been assigned to the imbalance in endo- and exo-cytosis,[69] which concerning podocytes could lead to disturbed secretion of glomerular matrix components impairing maintenance of glomerular basement membrane assembly. Interactions between endoplasmic reticulum and mitochondria were identified as key components of cellular function and disturbances in this connection are hallmarks of various disorders.[70] Ultrastructural changes in mitochondria and endoplasmic reticulum network due to excessive accumulation of MNP-SO-PEG in both types of cells corresponded to detected MNP-SO-PEG-induced inflammatory response. A comprehensive characterization of the underlying mechanisms of nanoparticle uptake and cellular responses need to be carried out in addition to understand in depth nano : bio interactions and so facilitate translation of nanoparticle-based platforms into clinics. Only studies considering multiple variables and performed on relevant cells are able to derive reliable conclusions on the potency of nanoparticles.

Conclusions

Our study demonstrates that under the same *in vitro* conditions, different cell types from the same tissue can react differently to the same nanomaterial. It also implies importance of surface chemistry as a driver of cell response to nanomaterials.

Conflicts of interest

There are no conflicts to declare.

Funding

This work was supported by the Slovak Research and Development Agency under the contract No. APVV-16-0579 and APVV-15-0215, by VEGA grants no. 2/0113/15 and 2/0094/15, and by the SASPRO Programme under Project No. 0084/01/02 and 0057/01/02, co-funded by the European Union FP7 and Marie-Curie Actions and the Slovak Academy of Sciences. This study was performed during the implementation of the project Building-up Centre for advanced materials application of the Slovak Academy of Sciences, ITMS project code 313021T081 supported by Research & Innovation Operational Programme funded by the ERDF. This paper is supported by European Union's Horizon 2020 research and innovation programme under grant agreement no 857381, project VISION (Strategies to strengthen scientific excellence and innovation capacity for early diagnosis of gastrointestinal cancers).

Acknowledgements

Authors would like to thank Dr M. Timko, Dr V. Zavisova, and Dr M. Koneracka from the Institute of Experimental Physics SAS, Kosice, for providing surface-modified MNPs and their characteristics after preparation. We would like to thank Dr B. Smolkova from the Cancer Research Institute BMC SAS for her valuable assistance with the statistics. Also, authors are grateful to MSc. N. Gregusova for excellent technical assistance and to L. Novota for technical assistance with electron microscopy.

References

1 Y. Li and R. A. Wingert, *Clin. Transl. Med.*, 2013, **2**, 11.
2 J. Danziger and M. P. Hoenig, *Am. J. Kidney Dis.*, 2016, **68**, 808.
3 A. Rodriguez-Barbero, B. L'azou, J. Cambar and J. M. Lopez-Novoa, *Cell Biol. Toxicol.*, 2000, **16**, 145.
4 C. A. Naughton, *Am. Fam. Physician*, 2008, **78**, 743.
5 H. Pavenstadt, W. Kriz and M. Kretzler, *Physiol. Rev.*, 2003, **83**, 253.
6 L. Schaefer, D. Mihalik, A. Babelova, M. Krzyzankova, H. J. Grone, R. V. Iozzo, M. F. Young, D. G. Seidler, G. Lin, D. P. Reinhardt and R. M. Schaefer, *Am. J. Pathol.*, 2004, **165**, 383.
7 S. Chen, B. Jim and F. N. Ziyadeh, *Semin. Nephrol.*, 2003, **23**, 532.
8 E. Ishimura, R. B. Sterzel, K. Budde and M. Kashgarian, *Am. J. Pathol.*, 1989, **134**, 843.
9 N. A. Wahab, L. Schaefer, B. S. Weston, O. Yiannikouris, A. Wright, A. Babelova, R. Schaefer and R. M. Mason, *Diabetologia*, 2005, **48**, 2650.
10 J. Reiser, W. Kriz, M. Kretzler and P. Mundel, *J. Am. Soc. Nephrol.*, 2000, **11**, 1.
11 G. Liu, B. Kaw, J. Kurfis, S. Rahmanuddin, Y. S. Kanwar and S. S. Chugh, *J. Clin. Invest.*, 2003, **112**, 209.
12 T. B. Huber and T. Benzing, *Curr. Opin. Nephrol. Hypertens.*, 2005, **14**, 211.
13 P. Mundel and J. Reiser, *Kidney Int.*, 2010, **77**, 571.
14 A. Babelova, F. Jansen, K. Sander, M. Lohn, L. Schafer, C. Fork, H. Ruetten, O. Plettenburg, H. Stark, C. Daniel, K. Amann, H. Pavenstadt, O. Jung and R. P. Brandes, *PloS One*, 2013, **8**, e80328.
15 F. C. Brosius, III, *Rev. Endocr. Metab. Disord.*, 2008, **9**, 245.
16 M. Longmire, P. L. Choyke and H. Kobayashi, *Nanomedicine*, 2008, **3**, 703.
17 L. Manil, J. C. Davin, C. Duchenne, C. Kubiak, J. Foidart, P. Couvreur and P. Mahieu, *Pharm. Res.*, 1994, **11**, 1160.
18 C. H. Choi, J. E. Zuckerman, P. Webster and M. E. Davis, *Proc. Natl. Acad. Sci. U.S.A.*, 2011, **108**, 6656.
19 H. S. Choi, W. Liu, F. Liu, K. Nasr, P. Misra, M. G. Bawendi and J. V. Frangioni, *Nat. Nanotechnol.*, 2010, **5**, 42.
20 X. Li, J. Wei, K. E. Aifantis, Y. Fan, Q. Feng, F. Z. Cui and F. Watari, *J. Biomed. Mater. Res.*, 2016, **104**, 1285.
21 I. Giouroudi and J. Kosel, *Recent Pat. Nanotechnol.*, 2010, **4**, 111.
22 J. Estelrich, M. J. Sanchez-Martin and M. A. Busquets, *Int. J. Nanomed.*, 2015, **10**, 1727.
23 P. Yang, F. Wang, X. Luo, Y. Zhang, J. Guo, W. Shi and C. Wang, *ACS Appl. Mater. Interfaces*, 2014, **6**, 12581.
24 K. Ulbrich, K. Hola, V. Subr, A. Bakandritsos, J. Tucek and R. Zboril, *Chem. Rev.*, 2016, **116**, 5338.
25 J. Xie, G. Liu, H. S. Eden, H. Ai and X. Chen, *Acc. Chem. Res.*, 2011, **44**, 883.

26 I. Celardo, J. Z. Pedersen, E. Traversa and L. Ghibelli, *Nanoscale*, 2011, **3**, 1411.
27 C. Farrera and B. Fadeel, *Eur. J. Pharm. Biopharm.*, 2015, **95**, 3.
28 M. Mesarosova, F. Ciampor, V. Zavisova, M. Koneracka, M. Ursinyova, K. Kozics, N. Tomasovicova, A. Hashim, I. Vavra, Z. Krizanova, Z. Husekova, M. Kubovcikova, P. Kopcansky, M. Timko and A. Gabelova, *Neoplasma*, 2012, **59**, 584.
29 M. Mesarosova, K. Kozics, A. Babelova, E. Regendova, M. Pastorek, D. Vnukova, B. Buliakova, F. Razga and A. Gabelova, *Toxicol. Lett.*, 2014, **226**, 303.
30 M. Takemoto, N. Asker, H. Gerhardt, A. Lundkvist, B. R. Johansson, Y. Saito and C. Betsholtz, *Am. J. Pathol.*, 2002, **161**, 799.
31 Q. Liu, Y. Wang and H. Thorlacius, *Biochem. Biophys. Res. Commun.*, 2000, **271**, 364.
32 Y. Li, Y. S. Kang, C. Dai, L. P. Kiss, X. Wen and Y. Liu, *Am. J. Pathol.*, 2008, **172**, 299.
33 J. Reiser and M. M. Altintas, *F1000Res.*, 2016, **5**, 114.
34 C. Alston-Roberts, R. Barallon, S. R. Bauer, J. Butler, A. Capes-Davis, W. G. Dirks, E. Elmore, M. Furtado, L. Kerrigan, M. C. Kline, A. Kohara, G. V. Los, R. A. MacLeod, J. R. Masters, M. Nardone, R. M. Nardone, R. W. Nims, P. J. Price, Y. A. Reid, J. Shewale, A. F. Steuer, D. R. Storts, G. Sykes, Z. Taraporewala and J. Thomson, *Nat. Rev. Canc.*, 2010, **10**, 441.
35 J. R. Lorsch, F. S. Collins and J. Lippincott-Schwartz, *Science*, 2014, **346**, 1452.
36 C. Pan, C. Kumar, S. Bohl, U. Klingmueller and M. Mann, *Mol. Cell. Proteomics*, 2009, **8**, 443.
37 C. S. Alge, S. M. Hauck, S. G. Priglinger, A. Kampik and M. Ueffing, *J. Proteome Res.*, 2006, **5**, 862.
38 J. F. Hillyer and R. M. Albrecht, *J. Pharm. Sci.*, 2001, **90**, 1927.
39 W. H. De Jong, W. I. Hagens, P. Krystek, M. C. Burger, A. J. Sips and R. E. Geertsma, *Biomaterials*, 2008, **29**, 1912.
40 M. Yu and J. Zheng, *ACS Nano*, 2015, **9**, 6655.
41 E. Calzoni, A. Cesaretti, A. Polchi, M. A. Di, B. Tancini and C. Emiliani, *J. Funct. Biomater.*, 2019, **10**(1), 4.
42 J. V. Jokerst, T. Lobovkina, R. N. Zare and S. S. Gambhir, *Nanomedicine*, 2011, **6**, 715.
43 J. S. Choi and N. Meghani, *Colloids Surf. B Biointerfaces*, 2016, **145**, 653.
44 A. O. Elzoghby, W. M. Samy and N. A. Elgindy, *J. Control. Release*, 2012, **157**, 168.
45 B. L'azou, J. Jorly, D. On, E. Sellier, F. Moisan, J. Fleury-Feith, J. Cambar, P. Brochard and C. Ohayon-Court, *Part. Fibre Toxicol.*, 2008, **5**, 22.
46 Z. Chen, H. Meng, G. Xing, C. Chen, Y. Zhao, G. Jia, T. Wang, H. Yuan, C. Ye, F. Zhao, Z. Chai, C. Zhu, X. Fang, B. Ma and L. Wan, *Toxicol. Lett.*, 2006, **163**, 109.
47 V. Kononenko, M. Narat and D. Drobne, *Arh. Hig. Rada. Toksikol.*, 2015, **66**, 97.
48 M. Nakayama, *Front. Immunol.*, 2018, **9**, 103.
49 Y. Totsuka, K. Ishino, T. Kato, S. Goto, Y. Tada, D. Nakae, M. Watanabe and K. Wakabayashi, *Nanomaterials*, 2014, **4**, 175.
50 E. A. Vermeij, M. I. Koenders, M. B. Bennink, L. A. Crowe, L. Maurizi, J. P. Vallee, H. Hofmann, W. B. van den Berg, P. L. van Lent and F. A. van de Loo, *PloS One*, 2015, **10**, e0126687.
51 O. Hauger, C. Delalande, H. Trillaud, C. Deminiere, B. Quesson, H. Kahn, J. Cambar, C. Combe and N. Grenier, *Magn. Reson. Med.*, 1999, **41**, 156.
52 Q. Y. Cai, H. Lee, E. J. Kim, H. Moon, K. Chang, J. Rho and K. S. Hong, *Nanomedicine*, 2012, **8**, 365.
53 C. H. Yeh, J. K. Hsiao, J. L. Wang and F. Sheu, *J. Nanoparticle Res.*, 2010, **12**, 151.
54 A. J. Schuerwegh, W. J. Stevens, C. H. Bridts and L. S. De Clerck, *Cytometry*, 2001, **46**, 172.
55 R. Berti, A. J. Williams, J. R. Moffett, S. L. Hale, L. C. Velarde, P. J. Elliott, C. Yao, J. R. Dave and F. C. Tortella, *J. Cereb. Blood Flow Metab. Suppl.*, 2002, **22**, 1068.
56 I. Lesur, J. Textoris, B. Loriod, C. Courbon, S. Garcia, M. Leone and C. Nguyen, *PloS One*, 2010, **5**, e11485.
57 Z. Deng, J. Jin, Z. Wang, Y. Wang, Q. Gao and J. Zhao, *Int. J. Nanomed.*, 2017, **12**, 3617.
58 V. Zavisova, M. Koneracka, A. Gabelova, B. Svitkova, M. Ursinyova, M. Kubovcikova, I. Antal, A. Jurikova, M. Molcan, M. Ognjanovic, B. Antic and P. Kopcansky, *J. Magn. Magn. Mater.*, 2020, **472**, 66.
59 K. Okamura, P. Dummer, J. Kopp, L. Qiu, M. Levi, S. Faubel and J. Blaine, *PloS One*, 2013, **8**, e54817.
60 D. Kerjaschki, *J. Clin. Invest.*, 2001, **108**, 1583.
61 M. Kretzler, I. Koeppen-Hagemann and W. Kriz, *Virchows Arch.*, 1994, **425**, 181.
62 S. Kim and J. Kwon, *J. Physiol.*, 2015, **593**, 1873.
63 B. Buliakova, M. Mesarosova, A. Babelova, M. Selc, V. Nemethova, L. Sebova, F. Razga, M. Ursinyova, I. Chalupa and A. Gabelova, *Nanomedicine*, 2017, **13**, 69.
64 V. Nemethova, B. Buliakova, P. Mazancova, A. Babelova, M. Selc, D. Moravcikova, L. Klescikova, M. Ursinyova, A. Gabelova and F. Razga, *Mater. Sci. Eng. C*, 2017, **70**, 161.
65 C. Colombo, M. Li, S. Watanabe, P. Messa, A. Edefonti, G. Montini, D. Moscatelli, M. P. Rastaldi and F. Cellesi, *ACS Omega*, 2017, **2**, 599.
66 A. Jochums, E. Friehs, F. Sambale, A. Lavrentieva, D. Bahnemann and T. Scheper, *Toxics*, 2017, **5**(3), 15.
67 D. Sahu, G. M. Kannan, M. Tailang and R. Vijayaraghavan, *J. Nanosci.*, 2016, 1.
68 F. Lazaro-Dieguez, N. Jimenez, H. Barth, A. J. Koster, J. Renau-Piqueras, J. L. Llopis, K. N. Burger and G. Egea, *Cell Motil. Cytoskeleton*, 2006, **63**, 778.
69 M. Misuth, J. Joniova, D. Horvath, L. Dzurova, Z. Nichtova, M. Novotova, P. Miskovsky, K. Stroffekova and V. Huntosova, *Cell. Signal.*, 2017, **34**, 11.
70 J. Li, D. Zhang, B. J. J. M. Brundel and M. Wiersma, *Cells*, 2019, **8**(12), 1617.